



Article

# Syntheses, Structures, and Photocatalytic and Sonocatalytic Degradations of Methyl Blue of Cu(II) and Mn(II) Coordination Polymers Based on Tri(triazole) and Dicarboxylate Ligands

 Chao Yin, Xing Wang, Jian-Gang Ding, Bao-Long Li , Bing Wu and Chuan-Jiang Hu 

College of Chemistry, Chemical Engineering, and Materials Science, Soochow University, Suzhou 215123, China; yinc@catl.com (C.Y.); 20224209136@stu.suda.edu.cn (X.W.); dingjiangang@suda.edu.cn (J.-G.D.); wubing@suda.edu.cn (B.W.); cjhu@suda.edu.cn (C.-J.H.)

\* Correspondence: libaolong@suda.edu.cn

**Abstract:** Cu(II) and Mn(II) coordination polymers  $[Cu(ttpa)(sub)]_n$  (**Cuttpa** or **1**) and  $[Mn_2(ttpa)_2(nip)_2(H_2O)_2] \cdot 3H_2O)_n$  (**Mnttpa** or **2**) (ttpa = tris(4-(1,2,4-triazol-1-yl)phenyl)amine,  $H_2sub$  = suberic acid, nip = 5-nitroisophthalate) were hydrothermally prepared and the structures were characterized. **Cuttpa** exhibited a 2D (4,4) network based on  $[Cu_2(COO)_4]$  dimers with upper and lower dangled ttpa ligands and a 2D  $\rightarrow$  3D polythreaded network. **Mnttpa** showed a 2D (4,4) network with dangled uncoordinated triazole rings from ttpa ligands and nitro groups from  $nip^{2-}$  ligands and a 2D  $\rightarrow$  3D polythreaded network.  $E_g$  data of **Cuttpa** and **Mnttpa** were 1.88 eV and 2.11 eV. **Cuttpa** and **Mnttpa** exhibited good catalytic activity for the decomposition of methyl blue (MB) under visible light and supersound irradiation. The decomposition mechanism using **Cuttpa** was explored. The holes ( $h^+$ ) and  $\bullet OH$  hydroxyl radicals played the main roles, and the  $\bullet O_2^-$  superoxide radicals played certain auxiliary roles in the decomposition of MB within the **Cuttpa** catalyst.

**Keywords:** coordination polymer; polythreaded; photocatalysis; sonocatalysis; catalytic mechanism



**Citation:** Yin, C.; Wang, X.; Ding, J.-G.; Li, B.-L.; Wu, B.; Hu, C.-J. Syntheses, Structures, and Photocatalytic and Sonocatalytic Degradations of Methyl Blue of Cu(II) and Mn(II) Coordination Polymers Based on Tri(triazole) and Dicarboxylate Ligands. *Molecules* **2024**, *29*, 5289. <https://doi.org/10.3390/molecules29225289>

Received: 12 October 2024

Revised: 3 November 2024

Accepted: 7 November 2024

Published: 8 November 2024



**Copyright:** © 2024 by the authors. Licensee MDPI, Basel, Switzerland. This article is an open access article distributed under the terms and conditions of the Creative Commons Attribution (CC BY) license (<https://creativecommons.org/licenses/by/4.0/>).

## 1. Introduction

In recent years, more and more inorganic chemistry and materials scientists have become interested in coordination polymers, not only due to their greatly varying and interesting structures [1], but also due to their multifunctional materials for use in applications such as chemical sensors [2], gas storage and adsorption [3], adsorbents for the elimination of toxic chemicals and pollutants [4], catalysis [5], magnetism [6], luminescence [7] and biology [8]. Entanglement is an important topic related to coordination polymers which usually allows for improvement in their packing efficiency when one single network has large free voids [9]. In addition to interpenetration, polycatenation and polyknots, polythreaded systems represent one more intriguing subgroup of entanglement [9–11]. Polythreaded frameworks are usually constructed from low-dimensional networks such as 0D, 1D and 2D networks with dangled side arms which are frequently assembled by longer organic ligands [9–11]. Even now, polythreaded systems are still less commonly explored. Examples of 2D  $\rightarrow$  3D polythreaded networks are scarcely documented [12–16].

With the population increasing and social development, the increasing prevalence of organic wastewater is a serious environmental topic. In the past two decades, the effective treatment of organic wastewater has been an important topic. Compared with other methods, such as membrane technology, coagulation and flocculation, to remove dyes from dirty water, photocatalysis has its own unique advantages, such as simple manipulation procedures, low energy consumption, no secondary pollution and high degradation efficiency, and it can use photocatalysts to degrade organic dyes into non-toxic small molecules with solar energy [17]. Nevertheless, the traditional inorganic semiconductor photocatalysts such as  $TiO_2$  and ZnO with high band gaps ( $E_g$ ) (3.2 eV for  $TiO_2$ , 3.4 eV for ZnO) only

could utilize a small amount of ultraviolet light (<4%) or visible light or sunlight from solar energy [18,19]. Sunlight contains approximately 45% visible light. Coordination polymer catalysts showing low band gaps could degrade organic dyes under visible light irradiation or sunlight with high efficiency [20–25]. This is one good example of utilizing solar energy. Meanwhile, the sonocatalytic degradation of organic dyes under ultrasound also is one good method of removing organic dyes [26].

The topologies and properties of coordination polymers are strongly dependent on central metal cations and ligands [27–30]. N-donor ligands (containing pyridine, triazole, imidazole) and O-donor carboxylate co-ligands are widely employed for constructing coordination polymers [27–30]. Tris(4-(1,2,4-triazol-1-yl)phenyl)amine (ttpa) contains three triazole rings around the triphenylamine center and can strongly coordinate to metal ions with its three four-position triazole N atoms [31–33]. Multicarboxylate ligands such as suberic acid ( $H_2sub$ ) and 5-nitroisophthalic acid ( $H_2nip$ ) containing two carboxylate groups can link metal ions with diverse coordination modes and can deprotonate to balance the charge of the coordination network [34,35]. Herein, copper(II) and manganese(II) coordination polymers,  $[Cu(ttpa)(sub)]_n$  (**Cuttpa** or **1**) and  $\{[Mn_2(ttpa)_2(nip)_2(H_2O)_2] \cdot 3H_2O\}_n$  (**Mnttpa** or **2**), were hydrothermally successfully prepared by employing the N-donor ligand ttpa and O-donor ligands  $H_2sub$  and  $H_2nip$ . Their structures were characterized. **Cuttpa** has a 2D (4,4) network with a  $Cu_2(COO)_4$  unit and a 2D  $\rightarrow$  3D polythreaded framework. **Mnttpa** has a 2D (4,4)-network and a 2D  $\rightarrow$  3D polythreaded framework. The catalytic decomposition of methyl blue (MB) under visible light and supersound irradiation were observed. The decomposition mechanism using **Cuttpa** was studied.

## 2. Results and Discussion

### 2.1. Structures

**Cuttpa** has a 2D (4,4)-network with a  $Cu_2(COO)_4$  unit and a 2D  $\rightarrow$  3D polythreaded framework. The **Cuttpa** crystal was monoclinic and  $P2_1/c$ . The unsymmetric units were the Cu(II) (Cu(1)), the ttpa, as well as the  $sub^{2-}$ . Cu(1) was in distorted square pyramidal coordination through four  $COO^-$  O atoms (O(1), O(2A), O(3B), O(4C)) of four  $sub^{2-}$  (Cu(1)-O(1) 1.962(3) Å; Cu(1)-O(2A) 1.984(3) Å; Cu(1)-O(3B) 1.969(2) Å; Cu(1)-O(4C) 1.965(2) Å) in the square plane and one triazole N atom (N(3)) of one ttpa (Cu(1)-N(3) 2.172(2) Å) at the axis (Figure 1a).

Each oxygen atom of two carboxylates from one  $sub^{2-}$  coordinates a copper(II) atom. A  $sub^{2-}$  connects four copper(II) atoms, forms a  $[Cu_2(COO)_4]$  unit, and assembles a  $[Cu(sub)]_n$  2D (4,4) network with a  $[Cu_2(COO)_4]$  unit (Figure 1b). The point symbol for this 2D network is  $4^4 \cdot 6^2$  [36].

The ttpa ligand contains three triazole rings based on the tris(phenyl)amine frame. But only a four-position triazole N (N3) of one ttpa ligand coordinates a copper(II) atom. Two other four-position triazole N atoms (N6, N9) do not coordinate. Therefore, uncoordinated triazole rings serve as dangling arms which are located above and below the  $[Cu(sub)]_n$  2D network (Figure 1c). The dangling arms thread into the windows of adjacent 2D networks and yield the 2D  $\rightarrow$  3D polythreaded framework (Figure 1d).

**Mnttpa** has a 2D (4,4)-network and a 2D  $\rightarrow$  3D polythreaded framework. Crystal **Mnttpa** is a triclinic crystal system and a  $P\bar{1}$  space group. The unsymmetric unit is two Mn(II) atoms (Mn(1), Mn(2)), two ttpa ligands, two  $nip^{2-}$  ligands, as well as two coordinated  $H_2O$  atoms (O(7), O(14)). The Mn(1) is in the distorted octahedral coordination with three carboxylate O atoms (O(1), O(10A), O(11A)) of two  $nip^{2-}$  ligands (Mn(1)-O(1) 2.1357(16) Å; Mn(1)-O(10A) 2.3936(17) Å; Mn(1)-O(11A) 2.2382(17) Å), one oxygen atom, O(7), of coordinated water (Mn(1)-O(7) 2.1469(17) Å), and two triazole N atoms (N(3), N(16B)) of two ttpa ligands (Mn(1)-N(3) 2.238(2) Å; Mn(1)-N(16B) 2.225(2) Å) (Figure 2a). The Mn(2) is in the distorted octahedral coordination with three  $COO^-$  O atoms (O(3), O(4), O(8)) of two  $nip^{2-}$  ligands (Mn(1)-O(3) 2.2362(17) Å; Mn(1)-O(4) 2.2340(17) Å; Mn(1)-O(8) 2.1537(17) Å), one oxygen atom, O(14), of coordinated water (Mn(1)-O(14) 2.1652(18) Å), and two triazole N atoms (N(6C), N(13)) of two ttpa ligands (Mn(1)-N(6C) 2.249(2) Å; Mn(1)-N(13) 2.247(2) Å) (Figure 2a).

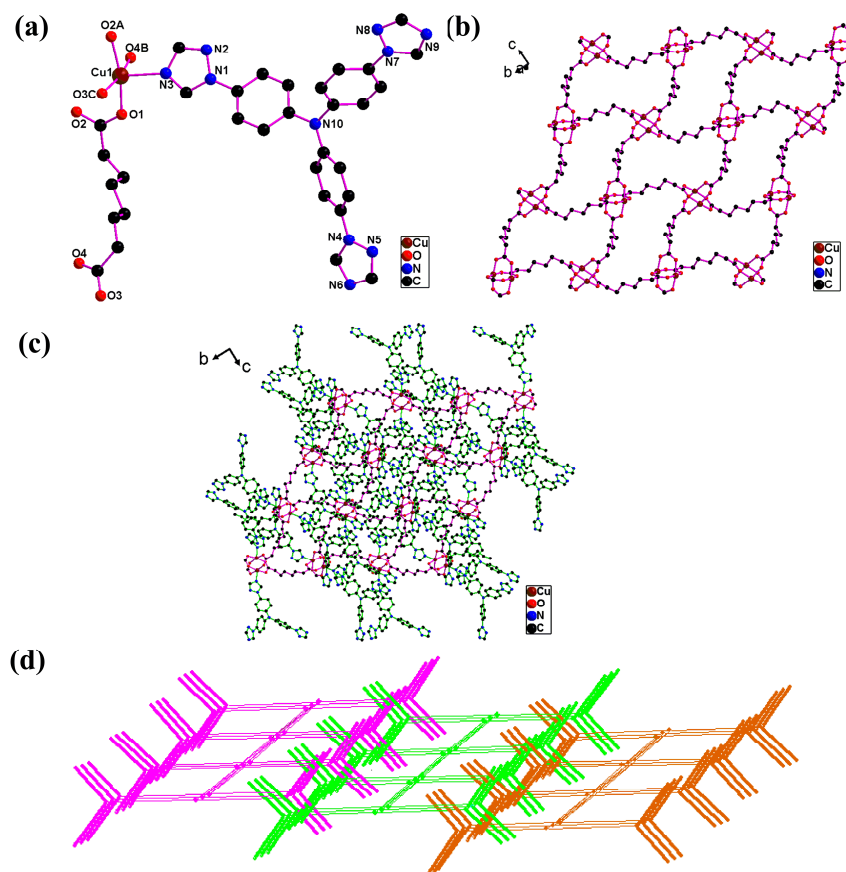


**Figure 1.** (a) The coordination of Cu(II) in *Cuttpa*. (b) The 2D network  $[Cu(sub)]_n$  in *Cuttpa*. (c) The 2D network  $[Cu(tpa)(sub)]_n$  in *Cuttpa*. (d) Scheme showing the 2D→3D polythreaded framework in *Cuttpa*.

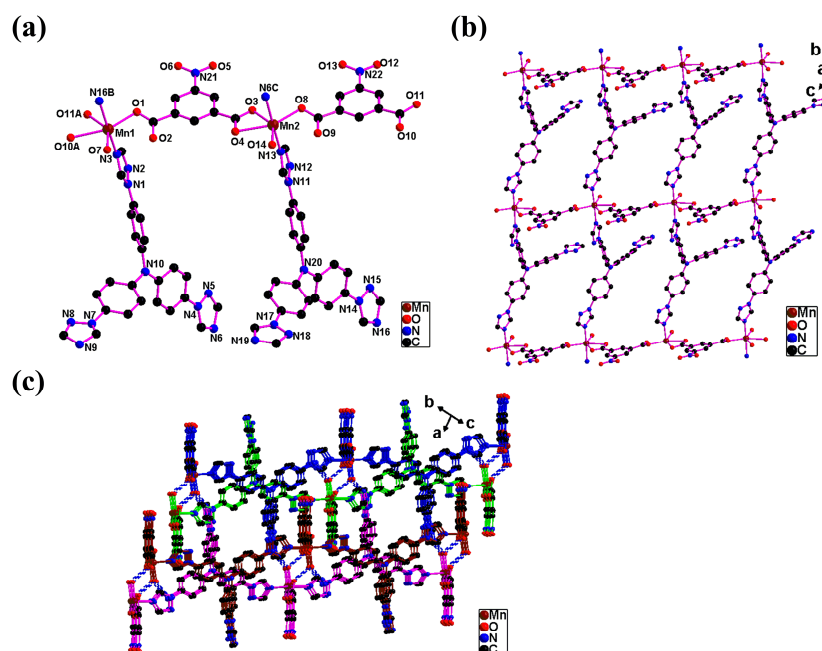


**Figure 2.** (a) The coordination Mn(II) atoms in *Mnttpa*. (b) The 2D network in *Mnttpa*. (c) The 2D→3D polythreaded framework in *Mnttpa*. The blue dashed lines present the hydrogen bonding interaction from adjacent 2D networks. The dashed lines show the hydrogen bonding interactions.

The carboxylate (O(1)O(2) or O(8)O(9)) of one  $\text{nip}^{2-}$  ligand exhibits monodentate. The other carboxylate (O(3)O(4) or O(10)O(11)) of one  $\text{nip}^{2-}$  ligand serves as a chelating coordinated mode (Figure 2a). Each  $\text{nip}^{2-}$  ligand behaves as a bridge and links two Mn(II) atoms. The ttpa ligand contains three triazole rings based on the tris(phenyl)amine frame. But two four-position triazole N atoms (N(3)N(6) or N(13)N(16)) of one ttpa ligand serve bridging functions and link two Mn(II) atoms. One other four-position triazole N (N(9) or N(19)) was uncoordinated. Therefore, the Mn(II) atoms are linked by  $\text{nip}^{2-}$  and ttpa bridging and assemble the 2D (4,4) network (Figure 2b). The point symbol of this 2D network is  $4^4 \cdot 6^2$  [36].

Therefore, uncoordinated triazole rings from the ttpa ligands and nitro groups from the  $\text{nip}^{2-}$  ligands serve as dangling arms which are located above and below the 2D network (Figure 2c). The dangling arms thread into the windows of adjacent 2D networks and yield a 2D  $\rightarrow$  3D polythreaded framework (Figure 2c). The hydrogen bond interactions between coordinated  $\text{H}_2\text{O}$  molecules and carboxyl O and triazole N atoms from adjacent 2D networks (O(7)...O(2) (1 - X, 1 - Y, -Z) 2.701(3) Å; O(7)...N(19) (-X, 1 - Y, -Z) 2.788(3) Å; O(14)...O(9) (1 - X, 2 - Y, 1 - Z) 2.675(3) Å; O(14)...N(9) (-X, 1 - Y, -Z) 2.834(3) Å) have important roles in the stability of 3D polythreaded supramolecular architecture (Figure 2c). A polythreaded framework is an interesting topic within crystal engineering [9–16]. The 2D  $\rightarrow$  3D polythreaded frameworks are uncommon, and few have been documented [12–16]. This research gave two new examples of 2D  $\rightarrow$  3D polythreaded frameworks.

## 2.2. Syntheses, PXRDs, FT-IR, and $E_g$

**Cuttpa** and **Mnttpa** were successfully synthesized by using ttpa,  $\text{H}_2\text{suc}$ , or  $\text{H}_2\text{nip}$  and Cu(II) or Mn(II) with the hydrothermal method. The reaction conditions (solvent  $\text{H}_2\text{O}/\text{DMF}$ , the reaction temperature, the ratio of reactants, and pH (the reactant NaOH)) were first employed according to our previous synthesis experience. The ratios of ttpa: $\text{H}_2\text{suc}$ :Cu(II) = 1:2:3 and ttpa: $\text{H}_2\text{nip}$ :Mn(II) = 1:2:3 were used due to the need to improve yield based on the expensive ttpa ligand. The reaction products from different reaction temperatures and different reaction times were observed. The different reaction temperatures and reaction times for syntheses of **Cuttpa** and **Mnttpa** were selected because of the high quality of single crystals suitable for single-crystal X-ray diffraction (91 °C and 3.1 days for the synthesis of **Cuttpa**; 101 °C and 2.2 days for the synthesis of **Mnttpa**) that were obtained for these reactions. Meanwhile, the synthesis of coordination polymers was not successful when using ttpa,  $\text{H}_2\text{nip}$ , and Cu(II). No coordination polymer was obtained by using ttpa,  $\text{H}_2\text{suc}$ , and Mn(II).

The powder X-ray diffraction (PXRD) patterns of **Cuttpa** and **Mnttpa** were recorded at room temperature (Figures S1 and S2). The peak positions of the simulated and experimental PXRD patterns are in agreement with each other, which confirms their phase purities.

The FT-IR spectra of **Cuttpa** and **Mnttpa** were recorded. For **Cuttpa**, the peaks at 1615, 1592, and 1495  $\text{cm}^{-1}$  are attributed to the asymmetric and symmetric stretching vibrations of carboxylate. There are no absorptions in the 1690~1730  $\text{cm}^{-1}$  region, indicating the complete deprotonation of  $\text{H}_2\text{suc}$  [34]. The peaks at 1515 and 1275  $\text{cm}^{-1}$  are attributed to the stretching vibration region of C=N bonds of the ttpa ligand. For **Mnttpa**, the broad absorption (3112  $\text{cm}^{-1}$ ) is due to the O-H group stretching vibration from the water molecules. The peaks at 1604, 1376, and 1349  $\text{cm}^{-1}$  are attributed to the asymmetric and symmetric stretching vibrations of carboxylate [34]. The peak at 1558  $\text{cm}^{-1}$  is attributed to the nitro group from  $\text{nip}^{2-}$ . The peaks at 1517 and 1274  $\text{cm}^{-1}$  are attributed to the stretching vibration region of C=N bonds of the ttpa ligand.

UV spectra for **Cuttpa** and **Mnttpa** showed that the  $E_g$  data of **Cuttpa** and **Mnttpa** were 1.88 and 2.11 eV, respectively (Figure 3).



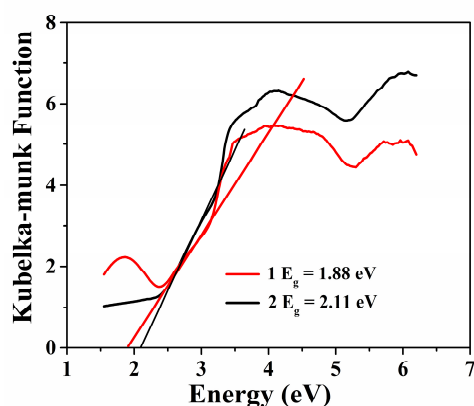


Figure 3. The UV spectra of **Cuttpa** (1) and **Mnttpa** (2).

### 2.3. Photocatalytic and Sonocatalytic Decomposition of MB

The photocatalytic and sonocatalytic decomposition of methyl blue (MB) was investigated within **Cuttpa** and **Mnttpa** catalysts under visible light and supersound irradiation. The decomposition efficiencies of trade  $\text{TiO}_2$  (60 nm) and  $\text{TiO}_2$  (20 nm) were also measured.

The decomposition efficiencies of MB were 92.5% within **Cuttpa**, 68.8% within **Mnttpa**, 38.2% within  $\text{TiO}_2$  (60 nm), 64.3% within  $\text{TiO}_2$  (20 nm), and 19.9% within blank  $\text{H}_2\text{O}_2$  within visible light after 90 min (Figures 4–6). After the photocatalytic decomposition experiments, **Cuttpa** and **Mnttpa** sustained their structures (Figures S1 and S2). The catalytic efficiency with decomposition MB was **Cuttpa** > **Mnttpa** >  $\text{TiO}_2$  (20 nm) >  $\text{TiO}_2$  (60 nm) within visible light. These results showed that **Cuttpa** is a good photocatalyst, and **Mnttpa** is an effective photocatalyst with the decomposition of MB.

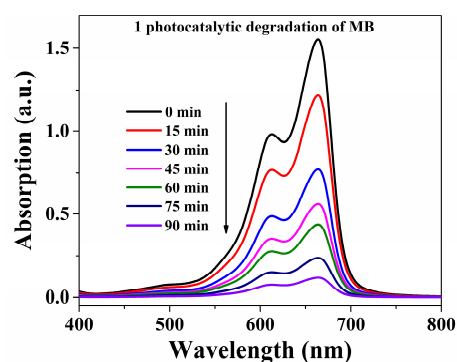


Figure 4. Absorption intensities for MB solution within photocatalytic process within **Cuttpa** (1) catalyst.

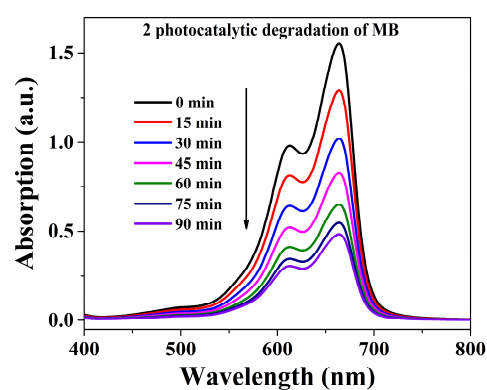
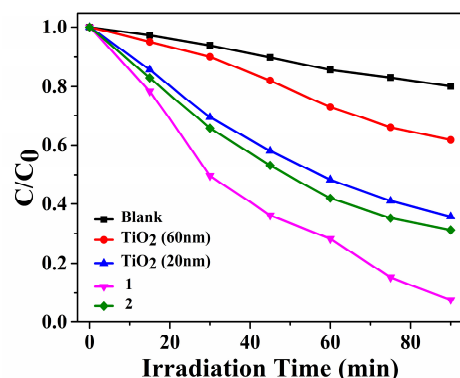
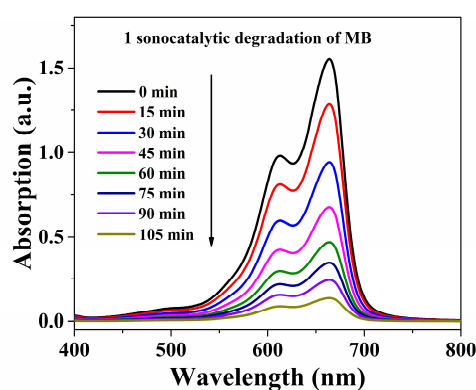


Figure 5. Absorption intensities for MB solution within photocatalytic process within **Mnttpa** (2) catalyst.



**Figure 6.** The decomposition efficiencies for MB within catalyst **Cuttpa** (1), **Mnttpa** (2), TiO<sub>2</sub>, and blank in the photocatalytic process.

The decomposition efficiencies with MB were 91.3% within **Cuttpa**, 54.9% within **Mnttpa**, 45.0% within TiO<sub>2</sub> (60 nm), 69.2% within TiO<sub>2</sub> (20 nm), and 22.8% within blank H<sub>2</sub>O<sub>2</sub> within ultrasound after 105 min (Figures 7–9). After the sonocatalytic decomposition experiments, **Cuttpa** and **Mnttpa** sustained their structures (Figures S1 and S2). The catalytic efficiency with the decomposition of MB was **Cuttpa** > TiO<sub>2</sub> (20 nm) > **Mnttpa** > TiO<sub>2</sub> (60 nm) within ultrasound. These experimental results showed that **Cuttpa** is a good sonocatalyst, and **Mnttpa** is an effective sonocatalyst for the decomposition of MB.



**Figure 7.** Absorption intensities of MB solution within sonocatalytic decomposition process within **Cuttpa** (1) catalyst.

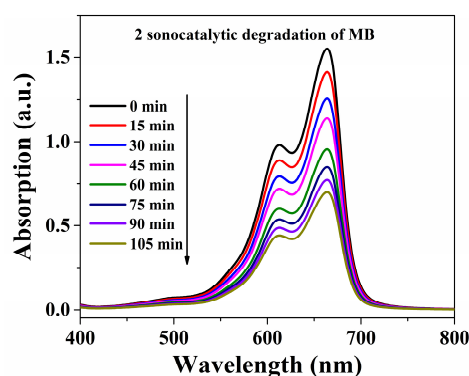


**Figure 8.** Absorption intensities of MB solution within sonocatalytic decomposition process within **Mnttpa** (2) catalyst.

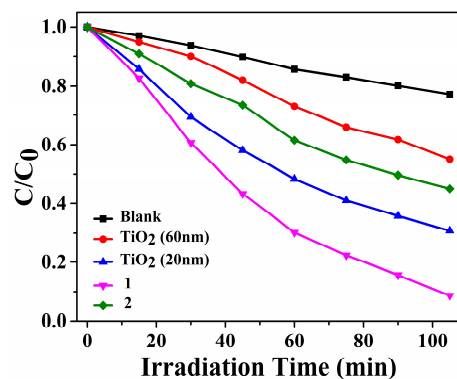


**Figure 9.** The decomposition efficiencies for MB within **Cuttpa** (1) and **Mnttpa** (2) catalysts and TiO<sub>2</sub> and blank in the sonocatalytic process.

The stability of the catalyst could be observed in the recycling experiments. After each cycling experiment, the **Cuttpa** (1) catalyst was recovered by centrifugation, filtration, washing with deionized water and ethanol several times, and then drying under room temperature. Figure 10 is a graph of five cycles of the photocatalytic degradation of MB by **Cuttpa** (1) under visible light irradiation. It can be seen that the catalytic activity decreased slightly after five cycles, and the final degradation efficiency reached 86.2% after five cycles. The suspension after the last cycle of the degradation experiment was taken out, centrifuged, and filtrated to give a clear solution. The amount of copper species in the solution was measured by ICP. The concentration of the copper species in the solution was low (0.13 mg/L). The removal rate of Cu(II) ions from the **Cuttpa** (1) catalyst was 0.35%, indicating the stable and reusable nature of the **Cuttpa** (1) catalyst.

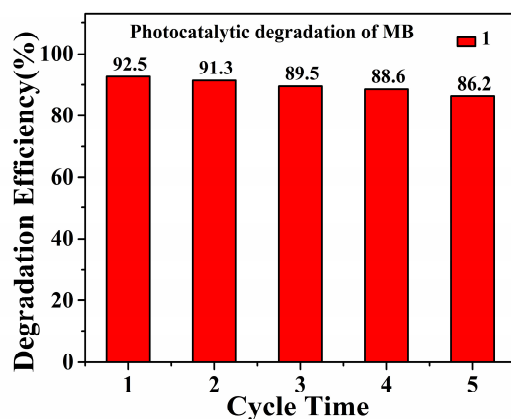


**Figure 10.** Five cycles of photocatalytic degradation of MB by **Cuttpa** (1) under the visible light irradiation.

The photocatalytic and sonocatalytic mechanisms are similar [37]. The photocatalytic experiments within **Cuttpa**, scavenger mannitol, benzoquinone (BQ), and ammonium oxalate (AO) were carried out (Figures 11 and 12). The decomposition efficiency of MB was 92.5% with **Cuttpa**. However, the decomposition efficiencies declined to 69.0% with BQ, 37.5% with mannitol, and 27.7% with AO. Here, the holes ( $h^+$ ) and  $\bullet OH$  hydroxyl radicals played the main roles, and the  $\bullet O_2^-$  superoxide radicals played certain auxiliary roles in the decomposition of MB within the **Cuttpa** catalyst.

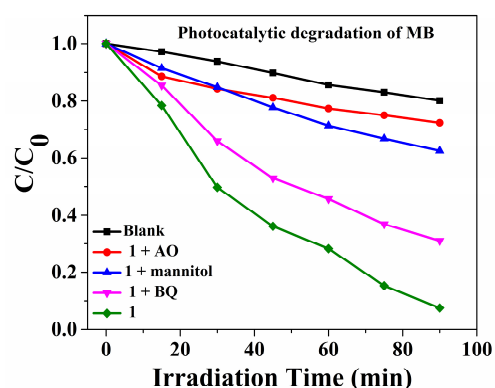


**Figure 11.** The decomposition efficiencies of MB with **Cuttpa** (1) and within the scavengers and blanks within the photocatalytic decomposition process.

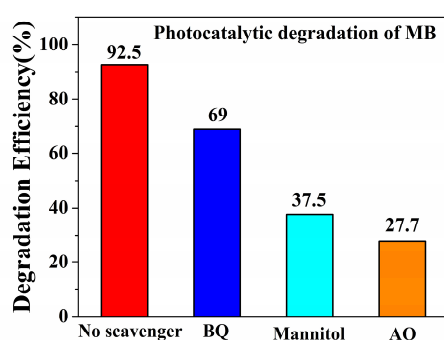


**Figure 12.** The decomposition efficiencies of MB with **Cuttpa** (1) and within the scavengers within the photocatalytic decomposition process.

The catalytic mechanism using **Cuttpa** and **Mnttpa** catalysts was supposed. When the **Cuttpa** or **Mnttpa** catalyst was exposed to visible radiation/supersound, the electrons of **Cuttpa** or **Mnttpa** could be emitted away from the valence band (VB) to the conduction band (CB), leading to the same amounts of holes ( $h^+$ ) in VB. The photoexcited electrons could react with  $H_2O_2$  to result in the  $\bullet OH$  hydroxyl radicals and react with oxygen and result in  $\bullet O_2^-$  superoxide. The holes ( $h^+$ ),  $\bullet OH$  hydroxyl, and  $\bullet O_2^-$  superoxide radicals perhaps decompose MB to result in  $CO_2$ ,  $H_2O$ , and other inorganic substances.

### 3. Experimental Section

#### 3.1. Materials and Methods

All other reagents were commercial and used without further purification. The spectra were measured on a Varian 1000 FT-IR spectrometer (Varian, Inc., Palo Alto, CA, USA) in the  $4000\text{--}400\text{ cm}^{-1}$  region. Powder X-ray diffractions (PXRDs) were performed using with a D2 Phaser (Bruker, Billerica, MA, USA) X-ray diffractometer with Cu-K $\alpha$  radiation ( $\lambda = 1.5406\text{ \AA}$ ) was used at room temperature. C, H and N were carried out on a Perkin-Elmer 240C analyser (Perkin-Elmer, Waltham, MA, USA). The UV-vis spectra were collected using a Cary 500 spectrometer (Agilent, Santa Clara, CA, USA). The amount of copper was measured using the inductively coupled plasma (ICP) spectrometer Optima 2100 (Perkin-Elmer, Ningbo, China).

#### 3.2. Preparation of $[Cu(tpa)(sub)]_n$ (**Cuttpa** or **1**)

The reactants of tpa (0.10 mmol, 0.045 g),  $H_2sub$  (0.20 mmol, 0.035 g),  $Cu(NO_3)_2 \cdot 3H_2O$  (0.30 mmol, 0.075 g), NaOH (0.037 mmol, 0.015 g),  $H_2O$  (3.6 mL), and DMF (1.7 mL) were placed into one hard glass tube (8.0 mL). The mixed reactants were heated to  $91\text{ }^\circ C$  for 3.1 days, and then chilled to  $19\text{ }^\circ C$ . The blue crystals  $[Cu(tpa)(sub)]_n$  were obtained and weighed as 0.038 g with a yield of 56% (based on tpa). Anal. Calc. for  $C_{32}H_{30}CuN_{10}O_4$

(**Cuttpa**): C, 56.34%; H, 4.43%; N, 20.54%. Found: C, 56.23%; H, 4.37%; N, 20.45%. IR data ( $\text{cm}^{-1}$ ): 1615 m, 1592 m, 1515 m, 1419 m, 1399 w, 1326 w, 1308 w, 1275 s, 1177 w, 1052 w, 978 m, 954 w, 833 m, 709 w, 654 m, 628 w.

### 3.3. Preparation of $\{[\text{Mn}_2(\text{ttpa})_2(\text{nip})_2(\text{H}_2\text{O})_2] \cdot 3\text{H}_2\text{O}\}_n$ (**Mnttpa** or 2)

The reactants of ttpa (0.10 mmol, 0.045 g),  $\text{H}_2\text{nip}$  (0.20 mmol, 0.042 g),  $\text{MnSO}_4 \cdot \text{H}_2\text{O}$  (0.030 mmol, 0.051 g), NaOH (0.037 mmol, 0.015 g),  $\text{H}_2\text{O}$  (3.6 mL), and DMF (1.7 mL) were placed into the hard glass tube (8.0 mL). The mixed reactants were heated to 101 °C for 2.2 days, and then chilled to 19 °C. The yellow crystals  $\{[\text{Mn}_2(\text{ttpa})_2(\text{nip})_2(\text{H}_2\text{O})_2] \cdot 3\text{H}_2\text{O}\}_n$  were obtained and weighed as 0.031 g with a yield of 41% (based on ttpa). Anal. Calc. for  $\text{C}_{64}\text{H}_{52}\text{Mn}_2\text{N}_{22}\text{O}_{17}$  (**Mnttpa**): C, 50.87%; H, 3.47%; N, 20.40%. Found: C, 50.72%; H, 3.41%; N, 20.29%. IR data ( $\text{cm}^{-1}$ ): 3112 m, 1604 m, 1558 m, 1517 s, 1451 w, 1434 w, 1376 m, 1349 m, 1274 m, 1145 w, 1113 m, 1081 w, 979 m, 832 w, 791 w, 733 m, 724 m, 673 m, 652 w.

### 3.4. X-Ray Crystallography

Crystal diffractions of  $[\text{Cu}(\text{ttpa})(\text{sub})]_n$  (**Cuttpa** or 1) and  $\{[\text{Mn}(\text{tpe})_2(\text{tpe})_2(\text{nip})_2(\text{H}_2\text{O})_2] \cdot 3\text{H}_2\text{O}\}_n$  (**Mnttpa** or 2) were explored with one Bruker APEX-II CCD. The structures were worked out and improved with the SHELXTL-2018 program [38]. The disordering lattice molecules of **Mnttpa** were omitted using PLATON (<https://www.platonsoft.nl/xraysoft/>, accessed on 6 November 2024). The crystallographic data are shown at Table 1. Important bond lengths and angles are presented in Table S1.

**Table 1.** Crystallographic data for **Cuttpa** and **Mnttpa**.

	<b>Cuttpa</b>	<b>Mnttpa</b>
Formula	$\text{C}_{32}\text{H}_{30}\text{CuN}_{10}\text{O}_4$	$\text{C}_{64}\text{H}_{46}\text{Mn}_2\text{N}_{22}\text{O}_{14}$
Fw	682.20	1457.11
T/K	188 (2)	189 (2)
Crystal system	Monoclinic	Triclinic
Space group	$P2_1/c$	$P\bar{1}$
$a/\text{Å}$	14.7579 (10)	11.5963 (8)
$b/\text{Å}$	18.6867 (13)	17.6243 (11)
$c/\text{Å}$	11.5203 (9)	19.6708 (12)
$\alpha$ (°)	90	113.519 (2)
$\beta$ (°)	100.047 (2)	94.839 (2)
$\gamma$ (°)	90	104.434 (2)
$V/\text{Å}^3$	3128.3 (4)	3492.6 (4)
$F(000)$	1412	1492
Z	4	2
$\rho_{\text{calcd}}$ ( $\text{g cm}^{-3}$ )	1.448	1.386
$\mu$ ( $\text{mm}^{-1}$ )	0.753	0.440
Reflections collected	60030	68,021
Unique reflections	7209 [R(int) = 0.0894]	15,953 [R(int) = 0.0951]
Parameter	424	939
Goodness of fit	1.050	1.050
$R_1$ [ $I > 2\sigma(I)$ ]	0.0541	0.0591
$wR_2$ (all data)	0.1519	0.1797

### 3.5. Photocatalytic and Sonocatalytic Decomposition

The photocatalytic experiment was carried out using a PCR-I multipurpose photoreactor (Beijing China Education Au-Light Company Limited, Beijing, China) equipped a CEL-HXF300 Xe lamp with a UV cut-off filter (providing visible light with  $\lambda > 400$  nm). The amounts 40 mg of catalyst (**Cuttpa** or **Mnttpa**, or trade  $\text{TiO}_2$  (60 nm), or trade  $\text{TiO}_2$  (20 nm)) and 0.50 mL of 30%  $\text{H}_2\text{O}_2$  were added into 100 mL of methylene blue (MB) solution (10 mg/L). The suspension solutions were stirred in dark conditions for about 30 min to ensure the complete equilibration of the adsorption/desorption of dyes on the photocatalyst surface. Then, the mixture was stirred continuously under visible light ir-



radiation. At a given interval, aliquots of the reaction mixtures were periodically taken, purified by centrifugation, and analyzed with a UV-vis spectrophotometer at an absorption wavelength of 664 nm for MB. In order to evaluate the reusability of the catalyst **Cuttpa** for MB degradation, recycling experiments were carried out.

The sonocatalytic experiment was carried out in an ultrasonic bath (KQ-200VDE, Kunshan, China) which was operated at a frequency of 100 kHz and with an effective power output of 100 W. The amounts of 40 mg of catalyst (**Cuttpa** or **Mnttpa**, or trade TiO<sub>2</sub> (60 nm), or trade TiO<sub>2</sub> (20 nm)) and 0.50 mL of 30% H<sub>2</sub>O<sub>2</sub> were added into 100 mL of methylene blue (MB) solution (10 mg/L). The suspension solutions were stirred in dark conditions for about 30 min to ensure the complete equilibration of the adsorption/desorption of dyes on the catalyst surface before ultrasonic irradiation was started. The entire catalytic sonication process took place at 26 ± 2 °C in the dark to prevent the influence of daily or ambient light. Then, the mixture was submitted for ultrasonic irradiation. At a given interval, aliquots of the reaction mixture were periodically taken, purified by centrifugation, and analyzed with a UV-vis spectrophotometer at an absorption wavelength of 664 nm for MB.

#### 4. Conclusions

The copper(II) and manganese(II) coordination polymers were prepared and characterized. **Cuttpa** exhibited a 2D (4,4)-network with [Cu<sub>2</sub>(COO)<sub>4</sub>] and a 2D → 3D polythreaded network. **Mnttpa** showed a 2D (4,4)-network and a 2D → 3D polythreaded network. The catalytic decomposition of methyl blue (MB) by visible light and supersound irradiation were observed. The decomposition mechanism using **Cuttpa** was studied. The holes (h<sup>+</sup>) and •OH hydroxyl radicals played the main role, and the •O<sub>2</sub><sup>−</sup> superoxide radicals played a certain auxiliary role in the decomposition of MB within the **Cuttpa** catalyst. **Cuttpa** and **Mnttpa** are good catalysts in the decomposition of MB within visible light and supersound.

**Supplementary Materials:** The following supporting information can be downloaded at <https://www.mdpi.com/article/10.3390/molecules29225289/s1>, Figure S1: PXRD patterns of the simulated and the measured of **Cuttpa** (1), and after photocatalytic and sonocatalytic degradation. Figure S2: PXRD patterns of the simulated and the measured of **Mnttpa** (2), and after photocatalytic and sonocatalytic degradation. Table S1: Selected bond lengths (Å) and angles (°) for **Cuttpa** and **Mnttpa**.

**Author Contributions:** C.Y.: Investigation, Data Curation, Writing—Original Draft. X.W.: Methodology. J.-G.D.: Conceptualization, Writing—Review. B.-L.L.: Supervision, Review and Editing, Funding Acquisition. B.W.: Instrument. C.-J.H.: Funding Acquisition. All authors have read and agreed to the published version of the manuscript.

**Funding:** This research was funded by the National Natural Science Foundation of China (22071169), the Priority Academic Program Development of Jiangsu Higher Education Institutions (PAPD), the State and Local Joint Engineering Laboratory for Functional Polymeric Materials, and the project of scientific and technological infrastructure of Suzhou (SZS201905).

**Institutional Review Board Statement:** No applicable.

**Informed Consent Statement:** Not applicable.

**Data Availability Statement:** The crystallographic data have been deposited in the Cambridge Crystallographic Data Center (CCDC) with CCDC numbers 2094503, 2094504 at July 2021. These data can be obtained free of charge, either from the CCDC via <https://www.ccdc.cam.ac.uk/structures> (accessed on 6 November 2024) or can be obtained from the corresponding authors upon request.

**Conflicts of Interest:** The authors declare no conflicts of interest.

#### References

1. Lin, Z.J.; Lü, J.; Hong, M.; Cao, R. Metal–organic frameworks based on flexible ligands (FL-MOFs): Structures and applications. *Chem. Soc. Rev.* **2014**, *43*, 5867–5895. [[CrossRef](#)] [[PubMed](#)]
2. Wang, D.K.; Chen, K.X.; Wang, M.; You, Y.J.; Zhou, X.H. A two-fold interpenetrated Zn-based coordination polymer for highly selective and sensitive detection of MnO<sub>4</sub><sup>−</sup>. *J. Mol. Struct.* **2021**, *1239*, 130486. [[CrossRef](#)]

3. Hong, W.H.; Perera, S.P.; Burrows, A.D. Manufacturing of metal-organic framework monoliths and their application in CO<sub>2</sub> adsorption. *Microporous Mesoporous Mater.* **2015**, *214*, 149–155. [[CrossRef](#)]
4. Ashouri, V.; Adib, K.; Nasrabadi, M.R.; Ghalkhani, M. Preparation of the extruded UiO-66-based Metal-Organic Framework for the diazinon removal from the real samples. *J. Mol. Struct.* **2021**, *1240*, 130607. [[CrossRef](#)]
5. Hashemian, S.; Sedrpoushan, A.; Eshbala, F.H. Co-Zeolite imidazolate frameworks (ZIF-9@Zeolite) as heterogeneous catalyst for alcohols oxidation. *Catal. Lett.* **2017**, *147*, 196–203. [[CrossRef](#)]
6. Wan, Q.Y.; Wakizaka, M.; Yamashita, M. Single-ion magnetism behaviors in lanthanide(III) based coordination frameworks. *Inorg. Chem. Front.* **2023**, *10*, 5212–5224. [[CrossRef](#)]
7. Butorlin, O.S.; Petrova, A.S.; Toikka, Y.N.; Kolesnikov, I.E.; Orlov, S.N.; Ryazantsev, M.N.; Bogachev, N.A.; Skripkin, Y.M.; Mereshchenko, A.S. The Structure and Optical Properties of Luminescent Europium Terephthalate Antenna Metal–Organic Frameworks Doped by Yttrium, Gadolinium, and Lanthanum Ions. *Molecules* **2024**, *29*, 3558. [[CrossRef](#)]
8. Kaur, H.; Mahanta, G.C.; Gupta, V.; Kukkar, D.; Tyagi, S. Synthesis and characterization of ZIF-8 nanoparticles for controlled release of 6-mercaptopurine drug. *J. Drug Del. Sci. Technol.* **2017**, *41*, 106–112. [[CrossRef](#)]
9. Carlucci, L.; Ciani, G.; Proserpio, D.M. Proserpio, polycatenation, polythreading and polyknotting in coordination network chemistry. *Coord. Chem. Rev.* **2003**, *246*, 247–289. [[CrossRef](#)]
10. Jiang, H.L.; Makal, T.A.; Zhou, H.C. Interpenetration control in metal–organic frameworks for functional applications. *Coord. Chem. Rev.* **2013**, *257*, 2232–2249. [[CrossRef](#)]
11. Cai, S.L.; Lu, L.; Shi, C.C.; Wang, J.; Sun, Y.C. Effect of ligand on the assembly of two entangled coordination polymers: Structures and photocatalytic properties. *Polyhedron* **2020**, *191*, 114804. [[CrossRef](#)]
12. Yang, J.; Yan, S.W.; Wang, X.; Xiao, D.R.; Zhang, H.Y.; Chi, X.L.; Zhang, J.L.; Wang, E.B. An unusual polythreaded coordination network self-assembled from 2D motifs with two distinct lateral arms. *Inorg. Chem. Commun.* **2013**, *38*, 100–103. [[CrossRef](#)]
13. Zhang, J.L.; Yang, J.; Wang, X.; Zhang, H.Y.; Chi, X.L.; Yang, Q.; Chen, Y.; Xiao, D.R. A series of polythreaded architectures based on a long flexible tetracarboxylate ligand and different N-donor ligands. *Inorg. Chim. Acta* **2016**, *447*, 66–76. [[CrossRef](#)]
14. Wang, K.B.; Wang, X.; Zhang, D.; Wang, H.J.; Wang, Z.K.; Zhao, M.Y.; Xi, R.; Wu, H.; Zheng, M.B. Interpenetrated nano-MOFs for ultrahigh-performance supercapacitors and excellent dye adsorption performance. *CrystEngComm* **2018**, *20*, 6940–6949. [[CrossRef](#)]
15. Zhao, F.H.; Guo, W.Y.; Guo, S.Y.; Li, S.Y.; Li, Z.L.; Yan, X.Q.; Jia, X.M.; Huang, L.W.; You, J.H. Two entangled photoluminescent MOFs of naphthalenedisulfonate and bis(benzimidazole) ligands for selective sensing of Fe<sup>3+</sup>. *J. Solid State Chem.* **2019**, *278*, 120926. [[CrossRef](#)]
16. Liu, J.D.; Wang, Z.K.; Bi, R.; Mao, F.F.; Wang, K.B.; Wu, H.; Wang, X. A polythreaded Mn<sup>II</sup>-MOF and its superperformances for dye adsorption and supercapacitors. *Inorg. Chem. Front.* **2020**, *7*, 718–730. [[CrossRef](#)]
17. Singh, A.; Singh, A.K.; Liu, J.Q.; Kumar, A. Syntheses, design strategies, and photocatalytic charge dynamics of metal–organic frameworks (MOFs): A catalyzed photo-degradation approach towards organic dyes. *Catal. Sci. Technol.* **2021**, *11*, 3946–3989. [[CrossRef](#)]
18. Zhang, Y.; Fan, W.; Du, H.Q.; Zhao, Y.W. Study on photocatalytic performance of TiO<sub>2</sub> and Fe<sup>3+</sup>/TiO<sub>2</sub> coatings. *Surf. Eng.* **2017**, *33*, 849–856. [[CrossRef](#)]
19. Baradaran, M.; Ghodsi, F.E.; Bittencourt, C.; Llobet, E. The role of Al concentration on improving the photocatalytic performance of nanostructured ZnO/ZnO:Al/ZnO multilayer thin films. *J. Alloys Compd.* **2019**, *788*, 289–301. [[CrossRef](#)]
20. Alvaro, M.; Carbonell, E.; Ferrer, B.; Xamena, F.X.L.; Garcia, H. Semiconductor behavior of a metal-organic framework (MOF). *Chem. Eur. J.* **2007**, *13*, 5106–5112. [[CrossRef](#)]
21. Lu, L.; Wang, J.; Shi, C.C.; Sun, Y.C.; Wu, W.P.; Pan, Y.; Muddassir, M. Four structural diversity MOF-photocatalysts readily prepared for the degradation of the methyl violet dye under UV-visible light. *New J. Chem.* **2021**, *45*, 551–560. [[CrossRef](#)]
22. Wu, Z.B.; Yuan, X.Z.; Zhang, J.; Wang, H.; Jiang, L.B.; Zeng, G.M. Photocatalytic decontamination of wastewater containing organic dyes by metal–organic frameworks and their derivatives. *ChemCatChem* **2017**, *9*, 41–64. [[CrossRef](#)]
23. Bala, S.; Bhattacharya, S.; Goswami, A.; Adhikary, A.; Konar, S.; Mondal, R. Designing functional metal–organic frameworks by imparting a hexanuclear copper-based secondary building unit specific properties: Structural correlation with magnetic and photocatalytic activity. *Cryst. Growth Des.* **2014**, *14*, 6391–6398. [[CrossRef](#)]
24. Dong, J.P.; Shi, Z.Z.; Li, B.; Wang, L.Y. Synthesis of a novel 2D zinc(II) metal–organic framework for photocatalytic degradation of organic dyes in water. *Dalton Trans.* **2019**, *48*, 17626–17632. [[CrossRef](#)]
25. Liu, X.X.; Lu, L.P.; Zhu, M.L.; Englert, U. Design and synthesis of three new copper coordination polymers: Efficient degradation of an organic dye at alkaline pH. *Dalton Trans.* **2021**, *50*, 13866–13876. [[CrossRef](#)]
26. Mosleh, S.; Rahimi, M.R.; Ghaedi, M.; Dashtian, K. Sonophotocatalytic degradation of trypan blue and vesuvine dyes in the presence of blue light active photocatalyst of Ag<sub>3</sub>PO<sub>4</sub>/Bi<sub>2</sub>S<sub>3</sub>-HKUST-1-MOF: Central composite optimization and synergistic effect study. *Ultrason. Sonochem.* **2016**, *32*, 387–397. [[CrossRef](#)]
27. Razavi, S.A.A.; Morsali, A. Linker functionalized metal-organic frameworks. *Coord. Chem. Rev.* **2019**, *399*, 213023. [[CrossRef](#)]
28. Zeng, B.X.; Zhang, Y.; Chen, Y.H.; Liu, G.P.; Li, Y.Z.; Chen, L.J.; Zhao, J.W. 3-D Antimonotungstate framework based on 2,6-H<sub>2</sub>pdca-connecting iron-cerium heterometallic Krebs-type polyoxotungstates for detecting small biomolecules. *Inorg. Chem.* **2021**, *60*, 2663–2671. [[CrossRef](#)]
29. Martín-García, Y.; Tapiador, J.; Orcajo, G.; Ayala, J.; Lago, A.B. [BMIM][X] ionic liquids supported on a pillared-layered metal–organic framework: Synthesis, characterization, and adsorption properties. *Molecules* **2024**, *29*, 3644. [[CrossRef](#)]

30. Elenkova, D.; Dimitrova, Y.; Tsvetkov, M.; Morgenstern, B.; Milanova, M.; Todorovsky, D.; Zaharieva, J. Investigation of the sensing properties of lanthanoid metal–organic frameworks (Ln-MOFs) with terephthalic acid. *Molecules* **2024**, *29*, 3713. [[CrossRef](#)]
31. Shi, Z.Z.; Pan, Z.R.; Jia, H.L.; Chen, S.G.; Qin, L.; Zheng, H.G. Zn(II)/Cd(II) terephthalate coordination polymers incorporating bi-, tri-, and tetraptopic phenylamine derivatives: Crystal structures and photoluminescent properties. *Cryst. Growth Des.* **2016**, *16*, 2747–2755. [[CrossRef](#)]
32. Qian, L.L.; Blatov, V.A.; Wang, Z.X.; Ding, J.G.; Zhu, L.M.; Li, K.; Li, B.L.; Wu, B. Sonochemical synthesis and characterization of four nanostructural nickel coordination polymers and photocatalytic degradation of methylene blue. *Ultrason. Sonochem.* **2019**, *56*, 213–228. [[CrossRef](#)] [[PubMed](#)]
33. Ngue, C.M.; Baskoro, F.; Wong, H.Q.; Yen, H.J.; Leung, M.K. Co- and Ni-based electroactive metal–organic frameworks for stable lithium storage: Electrochemical and charge-storage behavior in response to different metal centers. *Cryst. Growth Des.* **2022**, *22*, 5872–5882. [[CrossRef](#)]
34. Luo, G.G.; Wu, D.L.; Liu, L.; Wu, S.H.; Li, D.X.; Xiao, Z.J.; Dai, J.C. A novel 1D T5(0)A(2) water tape incorporated in the channel of the first 3D silver-suberate framework. *J. Mol. Struct.* **2012**, *1014*, 92–96. [[CrossRef](#)]
35. Dutta, B.; Ahmed, F.; Mir, M.H. Coordination polymers: A promising candidate for photo-responsive electronic device application. *Dalton Trans.* **2023**, *52*, 17084–17098. [[CrossRef](#)]
36. Blatov, V.A.; Shevchenko, A.P.; Proserpio, D.M. Applied topological analysis of crystal structures with the program package ToposPro. *Cryst. Growth Des.* **2014**, *14*, 3576–3586.
37. Siadatnasab, F.; Farhadi, S.; Khataee, A. Sonocatalytic performance of magnetically separable CuS/CoFe<sub>2</sub>O<sub>4</sub> nanohybrid for efficient degradation of organic dyes. *Ultrason. Sonochem.* **2018**, *44*, 359–367. [[CrossRef](#)]
38. Sheldrick, G.M. *SHELXTL-2016, Program for the Refinement of Crystal Structures from Diffraction Data*; University of Göttingen: Göttingen, Germany, 2016.

**Disclaimer/Publisher’s Note:** The statements, opinions and data contained in all publications are solely those of the individual author(s) and contributor(s) and not of MDPI and/or the editor(s). MDPI and/or the editor(s) disclaim responsibility for any injury to people or property resulting from any ideas, methods, instructions or products referred to in the content.